Scientific Data

https://doi.org/10.1038/s41597-026-06734-1

Article in Press

An EEG dataset with carbon wire loops in cognitive tasks and resting state inside and outside MR scanners

Received: 18 August 2025

Accepted: 27 January 2026

Cite this article as: Tsutsumi, M., Kishi, T., Ogawa, T. *et al.* An EEG dataset with carbon wire loops in cognitive tasks and resting state inside and outside MR scanners. *Sci Data* (2026). https://doi.org/10.1038/s41597-026-06734-1

Mizuki Tsutsumi, Tomohiko Kishi, Takeshi Ogawa, Toshikazu Kuroda, Reinmer J. Kobler & Motoaki Kawanabe

Title

An EEG dataset with carbon wire loops in cognitive tasks and resting state inside and outside MR scanners

Author list

Mizuki Tsutsumi[#], Tomohiko Kishi[#], Takeshi Ogawa[*], Toshikazu Kuroda[*], Reinmer J. Kobler, Motoaki Kawanabe

[#]These two authors equally contributed to this work.

Affiliations

Cognitive Mechanisms Laboratories, Advanced Telecommunications Research Institute International, 2-2-2, Hikaridai, Seika-cho, Soraku-gun, Kyoto 619-0288, Japan

***Corresponding author**

Takeshi Ogawa, Ph.D
Toshikazu Kuroda, Ph.D
Address: 2-2-2, Hikaridai, Seika cho, Soraku gun, Kyoto, 619 0288, Japan
Tel: +81-774-95-1413, +81-774-95-1031
Fax: +81-774-95-1236
E-mail: t.ogawa@atr.jp, t.kuroda@atr.jp

Abstract

We present a new dataset consisting of functional magnetic resonance imaging (fMRI) and electroencephalography (EEG) collected from 39 healthy adults in their twenties to forties while performing cognitive tasks (visual oddball and N-back tasks) in addition to resting state. These tasks took place both inside and outside an MR scanner (i.e., simultaneous EEG-fMRI and EEG-only, respectively), enabling direct comparisons across the different recording environments. Moreover, a subset of the participants was in two different MRI scanners, allowing for traveling-subject analyses. In both scanners, we used EEG caps equipped with carbon wire loops to measure motion and ballistocardiogram artifacts for their subsequent removal from raw EEG signals, resulting in a dataset of superior quality compared to previous studies. All the raw data are publicly available for facilitating multimodal neuroimaging research.

Background & summary

Electroencephalography (EEG) and functional magnetic resonance imaging (fMRI) are two widely-used noninvasive methods for measuring brain activities. EEG measures electrophysiological signals on the scalp, which reflect neural activities. fMRI measures signals related to blood flow, blood volume, and oxygen metabolism (blood-oxygenation-level-dependent, or BOLD signals) as an indirect measure of the neural activity[1] and there typically are hemodynamic delays of 3-6 s. Their simultaneous recording allows for the integration of high temporal resolutions of EEG and high spatial resolutions of fMRI in the analysis of brain activity. Consequently, simultaneous EEG-fMRI has been extensively studied in the last two decades[2, 3, 4].

Simultaneous EEG-fMRI often is associated with problems despite its potentials. First, EEG data suffer from serious contamination with noise. Not only that shield rooms are absent but also MR scanners themselves offer a noisy environment for EEG recording: i) gradient artifact (GA), which occur due to switching in the gradient system as it adjusts the magnetic field for phase/frequency encoding[5]; ii) the helium pump[6] and motion artifacts from head/body movements[7]; and iii) ballistocardiogram (BCG) artifact[8]. Among those, BCG likely is the most challenging noise for its similarity in amplitude to EEG and also for its spectral profile (approximately 1 Hz and its harmonics) overlapping with the delta, theta, and artifacts[9]. For example, average artifact subtraction (AAS) is widely used to reduce GA[5] and BCG[10]. This method takes advantage of the repetitive nature of GA and BCG artifacts by creating an average noise template that can be effectively subtracted. Another approach is the carbon-wire loop (CWL)[11], which helps removing motion and BCG artifacts by independently measuring these artifacts based on Faraday's law of induction[12].

Several simultaneous EEG-fMRI datasets have already been published (Table 1). Most of these datasets include experimental tasks using visual stimuli[13, 14], possibly because vision is little affected by loud sound in MR scanners. Some datasets also include tasks using auditory stimuli[15, 16]. However, there are few datasets that allow for a direct comparison of EEG recorded inside and outside the MR scanner[14, 17]. Moreover, CWL has been used for denoising only in a few datasets[18,11].

Table 1. A summary of EEG-fMRI dataset in previous research.

(Table 1. goes here)

In the present work, we provide a new dataset consisting of EEG and fMRI collected from 39 healthy adults in their twenties to forties while performing cognitive tasks (N-back and visual oddball tasks) in addition to resting state. This dataset has three advantages compared to extant datasets. First, these tasks took place both inside and outside an MR scanner, enabling direct comparisons across the different recording environments. Second, we used EEG caps equipped with CWLs to reduce artifacts arising from MR scanners. Third, a subset of the participants was in two different scanners, allowing for a traveling-subject analysis[23]. A portion of the data presented in this study was used in Kuroda et al. (2024)[24] to evaluate a novel noise-reduction method. The dataset is prepared in machine-readable BIDS (Brain Imaging Data Structure)[25, 26] format, ensuring the ease of analysis.

Methods

Participants

The protocol of this study was approved by the ATR Review Board Ethics Committee (IRB committee number: 18000062; application number: 167) and followed the Declaration of Helsinki. Participants were recruited through public advertisements in the local community with two recruitment criteria: 1) ages ranging from 20 to 49; and 2) no self-reported health issues. Initially, 41 participants were recruited but two of them were excluded: one due to illness and one due to a device failure. Consequently, the present dataset consisted of a total of 39 participants (19 men, 20 women; mean age: 29.0; *SD*: 9.35). Among them, 33 participants (16 men, 17 women; ages: 20-48 with a mean of 29.6; *SD*: 9.67) were assigned to a Prisma fit scanner (Prisma; Siemens, Erlangen, Germany) whereas 16 (8 men, 8 women, ages: 20-48 with a mean of 29.0; *SD*: 9.45) assigned to a Verio scanner(Siemens, Erlangen, Germany), resulting in 10 participants (5 men, 5 women, age: 20-48 with a mean of 32.8; *SD*: 11.31) assigned to both scanners.

All instructions were in Japanese and the participants provided written informed consent prior to participation. In the informed consent, they explicitly agreed to provide information on their age and gender, structural MRI data, functional MRI data, EEG data, and behavioral data from the experimental tasks. They also agreed for data sharing with other research institutions and for public release. All data were anonymized for protecting participant privacy, including removal of the facial part of structural MRI data.

Participants had two laboratory visits for each scanner with each visit starting with EEG recording

in a shield room (i.e., outside an MR scanner: EEG-only). Then simultaneous EEG-fMRI began shortly after that. Table 2 shows a summary of experimental schedules. It should be noted that, due to time constraints, some recordings planned for Day 1 had to be postponed to Day 2, resulting in some missing data. Moreover, some participants assigned to Verio had a few additional laboratory visits (see Supplemental Material for more details).

Table 2. A summary of simultaneous EEG-fMRI experimental schedules.

(Table 2. goes here)

Data acquisitions of EEG and fMRI

Experimental settings

EEG recordings outside MR scanners took place in a shield room. The walls of the shield room were made of copper mesh to block electromagnetic noise from the outside, with the interior dimensions of 145 cm wide, 185 cm long, and 210 cm high. The shield room was equipped with a table, comfortable chairs, two ceiling lights, and an air conditioner. On the table were a conventional keyboard and a Dell® computer monitor (34 cm x 60 cm). The center of the monitor was approximately at eye level when the participant was seated. A photosensor was mounted at the bottom-right corner of the monitor, being connected to a Stim Tracker (Cedrus® model ST-100) to record the actual time at which the stimuli were presented. The ceiling lights and the air conditioner were each covered with wire mesh boxes to minimize noise.

Simultaneous EEG-fMRI recordings were conducted in Prisma and Verio. In Prisma, visual stimuli were displayed on an opaque screen via a projector (Cannon Power Projector, WUX6000 at 60 Hz frame rate), being visible to participants through a small mirror attached to the head coil. A photosensor was mounted at the bottom-right corner of the screen. In Verio, visual stimuli were presented to participants as in Prisma, using a projector (JVC, DLA-X7) with 60Hz frame rate. A photosensor was mounted likewise. In both scanners, an MR-compatible response device (HHSC-1 × 4-D, Current Designs, Inc., Pennsylvania, USA) was used to record button presses.

EEG acquisition

EEG signals were recorded using MR-compatible EEG caps and amplifiers (BrainAmp MR plus, BrainAmp ExG MR, and BrainCap MR; Brain productsGmbH, Germany), with each cap having 63

EEG channels, one electrocardiogram (ECG) channel, and four CWL channels. An appropriate size of the cap (54, 56, and 58 cm) was selected for each participant.

The electrodes of EEG caps were placed on the scalp according to a modified International 10-20 system. The ground and reference electrodes were placed at AFz and FCz, respectively. The ECG electrode was positioned on the participant's back. Conductive gel (Abralyt HiCl, EASYCAP, Brain Products GmbH, Germany) was used to maintain the impedance of all electrodes below 10 kΩ throughout the experiment. Raw EEG signals were sampled at 5kHz. EEG and fMRI data were recorded simultaneously using hardware clock synchronization (SyncBox, BrainProducts, Germany). The MR scanner also sent trigger signals to mark the start time of each fMRI volume acquisition in the EEG data.

MRI data acquisition

MRI data were acquired with a multi-band sequence in 3T MAGNETOM Prisma fit, running the syngo MR VE11C/E software, with 64-channel head coils (Siemens, Erlangen, Germany). The scan protocol followed the Multimodel Harmonized MRI Imaging Protocol (HARP; see https://hbm.brainminds-beyond.jp/documents/protocol.html). For each participant, we obtained T1-weighted structural images (repetition time [TR] = 2500 ms, echo time [TE] = 2.18 ms, flip angle = 8 deg, inversion time = 1000 ms, matrix = 300 x 320, 224 sagittal slices, 0.8 mm isotropic) and T2-weighted structural images (TR = 3200 ms, TE = 564 ms, flip angle = 120 deg, matrix = 300 x 320, 224 sagittal slices, 0.8 mm isotropic) as well as fieldmaps (both posterior-to-anterior [PA] and anterior-to-posterior [AP] sequences; TR = 6100 ms, TE = 60 ms, flip angle = 90 deg, matrix = 86 x 86, 60 sagittal slices, 2.4 mm isotropic).

MRI data also were acquired with a single-band sequence in 3T MAGNETOM Verio, running the syngo MR VB19A software, with 12-channel head coils (Siemens, Erlangen, Germany). We obtained T1 -weighted structural images (TR = 2250 ms, TE = 3.06 ms, flip angle = 9 deg, inversion time = 900 ms, matrix = 256 x 256, 208 sagittal slices, 1.0 mm isotropic) for each participant. T2-weighted images and fieldmaps were not acquired in Verio for safety reasons. Table 3 summarizes the parameters for each echo-planar imaging (EPI).

(Table 3 goes here)

Task data/stimuli description

Recording took place during resting state with eyes open, a visual oddball task, and an N-back task. In the shield room, there was an approximately 2-min break between recordings, during which instructions for the next task were given. Inside the MR scanner, there was a 40-s pre-task period and

a 30-s post-task period for each recording, during which a fixation cross was displayed. These additional periods were to stabilize the magnetic field in the MR scanner and also to create a template for removing GA in a subsequent process. A Panasonic® laptop computer with Python 3.9 controlled all experimental tasks. All visual stimuli were displayed in dark bluish/greenish colors (RGB: 47, 79, 79) on a black background.

Resting state

Participants were instructed to stare blankly at a fixation cross ("+") in the center of the screen without thinking anything and sleeping. The task lasted for eight minutes.

Visual oddball task

This task consisted of 250 trials, with each trial lasting for 1300 ms. Each trial had 650-ms pre-stimulus period (plus a jitter randomly selected from from -100 ms to 100 ms in steps of 2 ms), a stimulus presentation for 250 ms, and 450-ms post-stimulus period (minus the pre-stimulus jitter to keep trial duration constant) in this order. Two types of stimuli were presented: target and normal. A circle image was presented as a normal stimulus at $p = .8$ on average across participants, and a star image as a target stimulus at $p = .2$ on average. Each shape image was 125 px by 125 px in size. The actual number of trials with the target stimulus varied randomly between 47 and 53 in steps of 1. After the task, participants were asked to verbally report how many times the target stimulus was presented to ensure that they were attending to the task (but without penalty for incorrect answers). A fixation cross was displayed in the center of the screen during the pre-stimulus and post-stimulus periods.

N-back task

An N-back task consisted of two conditions: 0- and 2-back conditions. The stimulus was a single number (0-back: ranging from 0 to 9; ranging from 2-back: 1 to 9). Each condition was in effect twice, constituting one EEG recording. The order of the conditions was randomized for each recording. Each condition consisted of 60 trials, each lasting for 1500 ms. Each trial had a 10-ms pre-stimulus period, a stimulus presentation for 500 ms, and a 990-ms post-stimulus period in this order. In the 0-back condition, participants were instructed to press a button when the number "0" appeared on the screen. In the 2-back condition, participants were instructed to press a button when the number on the screen matched the number displayed two trials ago. In both conditions, a button press was considered valid and thus registered if it occurred sometime between 150 and 1400 ms after the stimulus onset. A fixation cross was displayed in the center of the screen during the pre-stimulus and post-stimulus periods.

EEG preprocessing

We used a pipeline that automatically preprocessed EEG data collected both inside and outside the MR scanner, taking steps described in Table 4. Some of the steps differed depending on whether EEG was acquired inside or outside the scanner as described below. All EEG files were converted to EEGLAB format[26] from step 7 onward.

Outside the MR scanner

For EEG recorded outside the MR scanner, we first applied a band-pass filter (0.5–125 Hz; Butterworth filter, second order, applied bidirectionally) and resampled the data to 250 Hz. We then used *autoreject* ver.0.4.0 (https://autoreject.github.io/stable/index.html)[28] to detect and interpolate noisy channels. *Autoreject* is an automatic data-driven algorithm that estimates optimal peak-to-peak thresholds for each datum, followed by detection and interpolation of abnormal segments. We also applied the RANSAC algorithm[29] to identify channels containing data that significantly deviated from those of other channels. Next, we removed power line noise (60 Hz) and re-referenced the data to a common average reference. After removing artifacts related to electrooculogram (EOG), we segmented the data into 10-s windows and performed artifact correction with *autoreject* using a sliding window method.

Inside the MR scanner

For EEG recorded simultaneously with fMRI, we first applied a high-pass filter (0.5 Hz, Butterworth filter, second order, applied bidirectionally). Next, we removed GA and BCG artifacts using AAS[5]. During this step, we used the FMRIB plug-in for EEGLAB, provided by the University of Oxford Centre for Functional MRI of the Brain (FMRIB)[30, 31]. We then applied a low-pass filter (0.5 Hz, Butterworth filter, second order, applied bidirectionally), resampled the data to 500 Hz, and applied CWL regression (https://github.com/jnvandermeer/CWRegrTool) [11] to reduce motion artifacts. The data were then resampled again to 250 Hz. As with EEG recorded outside the scanner, we detected and interpolated noisy channels, removed power line noise, re-referenced the data to a common average reference, removed EOG-related artifacts, segmented the data into 10-s windows, and performed artifact correction with *autoreject* using a sliding window method. Finally, we further attenuated residual BCG artifacts using generalized optimal basis set (OBS) – a custom method described by Kuroda et al. (2024)[24].

(Table 4 goes here)

MRI preprocessing

We used BIDS_spm_preprocessing script (https://github.com/kfinc/bids-spm-preprocessing) to process fMRI data. This script was designed for group-level SPM preprocessing of BIDS longitudinal data. We processed the data using SPM12 software as follows: (i) A first few volumes were discarded (12 and 4 volumes for Prisma and Verio, respectively) to allow for T1 equilibration; (ii) the remaining data were corrected for slice timing; (iii) the mean image of the sequence was realigned to compensate for head motion; (iv) the structural image was co-registered to the mean of the functional images and segmented into three tissue classes in Montreal Neurological Institute (MNI) space; (v) the functional images were normalized using the associated parameters and resampled onto a 2 × 2 × 2 mm grid; and (vi) the data were spatially smoothed using an isotropic Gaussian kernel with an 8 mm full width at half maximum.

Data quality control

Participants had to complete two laboratory visits to be included in the present dataset. Two participants were unable to complete due to either sickness or device failure. Body movement was not considered as an exclusion criterion. These criteria resulted in a total of 39 participants in the final set of data. It should be noted that we attempted to preprocess this dataset using fMRIPrep[32], but it did not work properly for the defaced sub-38 data. However, we confirmed successful preprocessing of this data with SPM12; thus, being included in this dataset.

Data privacy

All imaging data in this study have been anonymized by deleting personal information, except for sex and age. The T1-weighted structural image was defaced using the method proposed by Tanaka et al. (2021)[33]. However, as this method was insufficient for two participants assigned to Verio, we applied *fsl_deface*[34] to their T-1 structural images. For T2-weighted structural images in Prisma, *deface_T12*[85] was used. We carefully confirmed that the defaced T1 and T2 images showed no removal of gray matter through visual inspection.

Data records

Data organization

All data in this study have been organized following the BIDS format[36]. The dataset consists of raw

data for EEG data, EPI, and fieldmaps, and defaced data for T1-weighted image and T2-weighted image.

The provided link for the present dataset contains two main data folders, '41_prisma_deface' and '41_verio_deface', each following the BIDS standard. In each subject's folder, two session folders are included (Day 1: ses-1 and Day 2: ses-2), with a consistent structure across sessions. Specifically, each session folder contains (i) an 'anat' folder for structural MRI images, (ii) an 'eeg' folder for EEG data, (iii) a 'func' folder for fMRI data, and (iv) an 'fmap' folder for fieldmaps. MRI data are provided in the NIfTI format (.nii.gz), and EEG data are in the EEGLAB (.set) format. All datasets are raw but de-identified, and structural and functional MRI scans have been defaced (i.e., facial parts removed) to protect participant privacy. JSON files are included to provide acquisition parameters as metadata. All experimental events were recorded in the EEG file with their markers and descriptions described in the accompanying documentation file (event_marker_info.txt).

Technical Validation

EEG data validation and quality

To assess the quality of resting EEG data, we compared the power spectral density (PSD) of EEG signals after GA correction (GA), CWL regression (EEG-fMRI (preprocessed)), and autoreject (EEG-fMRI with autoreject) (Fig. 1). Just for the data presentation here, the frequency band was adjusted to 1-120 Hz at step 7 in Table 3. The frequency band of notable noise differed across MR scanners. When comparing results of GA to EEG-fMRI(preprocessed), with the main difference being the presence of CWL regression in the latter (see Table 4), noise in the 20–60 Hz range was considerably reduced in Prisma whereas noise in the 80–100 Hz range was reduced in Verio. These frequency ranges likely correspond to vibrations from the helium pump operation[24, 6, 8] in respective scanners. Thus, CWLs were effective in reducing motion-related artifacts. Additionally, CWL regression also reduced power at low frequencies. In both Prisma and Verio, artifact removal using *autoreject* led to an overall reduction in power for both simultaneous EEG-fMRI and EEG-only recordings. For EEG-only, the alternating current power at 60 Hz was effectively removed. As a result of these noise reductions, the final PSDs were similar to each other between simultaneous EEG-fMRI and EEG-only.

(Fig. 1 goes here)

Fig. 2 shows representative traces of all EEG channels for a single participant across different noise-reduction methods. The top two panels show EEG acquired inside the MRI scanner with noise removed (EEG-fMRI [GA] and EEG-fMRI[preprocessed]), whereas the bottom panel shows EEG outside the MRI scanner that has undergone preprocessing (EEG-only [preprocessed]). Compared to EEG-fMRI [GA], its combination with CWL regression considerably reduced noise.

(Fig. 2 goes here)

Next, we examined event-related potentials (ERPs) in oddball and N-back tasks. Fig. 3, 4, 5, and 6 show the ERPs averaged across subjects in each task separately for Prisma and Verio for EEG-only with autoreject and simultaneous EEG-fMRI with autoreject. In the oddball task (Figs 3 and 4), EEG signals from simultaneous EEG-fMRI showed physiologically meaningful signals such as P300 when comparing trials with target and normal stimuli although their overall amplitudes were smaller relative to EEG-only. Likewise, in the N-back task, physiologically meaningful signals such as P300 were observed for both simultaneous EEG-fMRI and EEG-only when comparing trials with match and normal stimuli, particularly in the 0-back condition (Figs 5 and 6). Results were similar in 2-back conditions but their amplitudes were much smaller than 0-back conditions possibly due to the increase in task difficulty[37].

(Fig. 3 goes here)

(Fig. 4 goes here)

(Fig. 5 goes here)

(Fig. 6 goes here)

fMRI data validation and quality

To assess the quality of fMRI data, we examined statistical differences in brain activity during experimental tasks. A general linear model (GLM) was applied using an event-related design (Table 5-8). For oddball, fMRI data were modeled with two regressors of interest (i.e., target and normal trials). For N-back, the data were modeled with four regressors of interest corresponding to the trial/condition

types (match_zero and non-match_zero respectively represent trials with match and non-match stimuli in the 0-back condition; match_two and non-match_two represent the respective stimuli in the 2-back condition). To localize the activated brain regions, we calculated contrast images for the following comparisons: (i) target > normal; (ii) match_zero > non-match_zero; (iii) match_two > non-match_two. We applied the contrast images as the input to group-level random-effect analysis with one-sample t-tests. The threshold for statistical significance was set at < 0.001 (uncorrected p-value) and a cluster-based family-wise-error correction of p-value < 0.05.

Although activation levels and spatial extent differed between the two scanners, the location of activation generally were consistent and related to common areas in previous research (e.g., visual oddball task: supplementary motor area[38]; N-back task: Lobule VI of cerebellar hemisphere[39]). Additionally, fMRI images (Supplementary Figure S5, S6) show similar results to previous research[38, 39]. The coordinates of the peak voxels of the clusters were similar between the two scanners but with larger t-values and cluster sizes in Prisma compared to Verio.

Table 5. Results of the contrast between target and normal stimuli in the visual oddball task in Prisma.

(Table 5. goes here)

Table 6. Results of contrasts for different combinations of match and non-match stimuli in 0- and 2-back conditions in the N-back task in Prisma.

(Table 6. goes here)

Table 7. Results of the contrast between target and normal stimuli in the visual oddball task in Verio.

(Table 7. goes here)

Table 8. Results of the contrast between match and non-match stimuli in 0- and 2-back conditions each in the N-back task in Verio.

(Table 8. goes here)

Code availability

MATLAB and Python codes for EEG preprocessing described in Table 4 are available from a link to our data repository after registering on our website, https://doi.org/10.34860/atr-EfP-2025.

Data availability

The datasets in this study are available through our website(https://doi.org/10.34860/atr-EfP-2025). Access to the data is provided to researchers upon registration, after which a link to the data repository will be supplied.

References

1. Buxton, R. B. *Introduction to functional magnetic resonance imaging*. https://doi.org/10.1017/CBO9780511549854 (Cambridge Univ. Press, 2002).
2. Britz, J., Van De Ville, D. & Michel, C. M. BOLD correlates of EEG topography reveal rapid resting-state network dynamics. *NeuroImage* **52**, 1162–1170 https://doi.org/10.1016/j.neuroimage.2010.02.052 (2010).
3. Mantini, D., Perrucci, M. G., Del Gratta, C., Romani, G. L. & Corbetta, M. Electrophysiological signatures of resting state networks in the human brain. *PNAS* **104**, 13170–13175 https://doi.org/10.1073/pnas.0700668104 (2007).
4. Jorge, J., van der Zwaag, W. & Figueiredo, P. EEG–fMRI integration for the study of human brain function. *NeuroImage* **102**, 24–34 https://doi.org/10.1016/j.neuroimage.2013.05.114 (2014).
5. Allen, P. J., Josephs, O. & Turner, R. A Method for Removing Imaging Artifact from Continuous EEG Recorded during Functional MRI. *NeuroImage* **12**, 230–239 https://doi.org/10.1006/nimg.2000.0599 (2000).
6. Rothlübbers, S. *et al.* Characterisation and Reduction of the EEG Artefact Caused by the Helium

Cooling Pump in the MR Environment: Validation in Epilepsy Patient Data. *Brain Topogr* **28**, 208–220 https://doi.org/10.1007/s10548-014-0408-0 (2015).

7. Hoffmann S. & Falkenstein M. The Correction of Eye Blink Artefacts in the EEG: A Comparison of Two Prominent Methods. *PLOS ONE* **3**, e3004 https://doi.org/10.1371/journal.pone.0003004 (2008).
8. Debener, S., Mullinger, J. K., Niazy, R. K. & Bowtel, R. W. Properties of the ballistocardiogram artefact as revealed by EEG recordings at 1.5, 3 and 7 T static magnetic field strength. *Int J Psychophysiol*, **67**, 189–199 https://doi.org/10.1016/j.ijpsycho.2007.05.015 (2008).
9. Abreu, R., Jorge, J., & Figueiredo, P. EEG quality: The pulse artifact. In C. Muler & L. Lemieux (Eds.), *EEG-fMRI: Physiological basis, technique, and applications* (pp. 167-188). (Springer, 2022).
10. Allen, P. J., Polizzi, G., Krakow, K., Fish, D. R. & Lemieux, L. Identification of EEG Events in the MR Scanner: The Problem of Pulse Artifact and a Method for Its Subtraction. *NeuroImage* **8**, 229–239 https://doi.org/10.1006/nimg.1998.0361 (1998).
11. van der Meer, J. N. *et al.* Carbon-wire loop based artifact correction outperforms post-processing EEG/fMRI corrections—A validation of a real-time simultaneous EEG/fMRI correction method. *NeuroImage* **125**, 880–894 https://doi.org/10.1016/j.neuroimage.2015.10.064 (2016).
12. Jorge, J., Grouiller, F., Gruetter, R., van der Zwaag, W. & Figueiredo, P. Towards high-quality simultaneous EEG-fMRI at 7 T: Detection and reduction of EEG artifacts due to head motion. *NeuroImage* **120**, 143–153 https://doi.org/10.1016/j.neuroimage.2015.07.020 (2015).
13. Telesford, Q. K. *et al.* An open-access dataset of naturalistic viewing using simultaneous EEG-fMRI. *Sci. Data* **10**, 554 https://doi.org/10.1038/s41597-023-02458-8 (2023).
14. Schrooten, M., Vandenberghe, R., Peeters, R. & Dupont, P. Quantitative Analyses Help in Choosing Between Simultaneous vs. Separate EEG and fMRI. *Front. Neurosci.* **12**, https://doi.org/10.3389/fnins.2018.01009 (2019).
15. He, H., Hong, L. & Sajda, P. Pupillary response is associated with the reset and switching of functional brain networks during salience processing. PLoS Comput. Biol **19**, e1011081 https://doi.org/10.1371/journal.pcbi.1011081 (2023).
16. Walz, J. M. *et al.* Prestimulus EEG alpha oscillations modulate task-related fMRI BOLD responses to auditory stimuli. *NeuroImage* **113**, 153–163 https://doi.org/10.1016/j.neuroimage.2015.03.028 (2015).
17. Georgie, Y. K., Porcaro, C., Mayhew, S. D., Bagshaw, A. P. & Ostwald, D. A perceptual decision making EEG/fMRI data set. 253047 Preprint at https://doi.org/10.1101/253047 (2018).
18. Kraljič, A., Matkovič, A., Purg, N., Demšar, J. & Repovš, G. Evaluation and comparison of most prevalent artifact reduction methods for EEG acquired simultaneously with fMRI. *Front.*

Neuroimaging **1**, https://doi.org/10.3389/fnimg.2022.968363 (2022).

19. Lioi, G., Cury, C., Perronnet, L., Mano, M., Bannier, E., Lécuyer, A. & Barillot, C. Simultaneous EEG-fMRI during a neurofeedback task, a brain imaging dataset for multimodal data integration. *Sci. Data* **7**, 173 https://doi.org/10.1038/s41597-020-0498-3 (2020).
20. Gu, Y., Sainburg, L. E., Han, F. & Liu, X. Simultaneous EEG and functional MRI data during rest and sleep from humans. *Data in Brief* **48**, 1-5 https://doi.org/10.1016/j.dib.2023.109059 (2023).
21. Daly, I., Williams, D., Hwang, F., Kirke, A., Miranda, E. R. & Nasuto, S. J. Electroencephalography reflects the activity of sub-cortical brain regions during approach-withdrawal behaviour while listening to music. *Sci. Rep*, **9**, 9415 https://doi.org/10.1038/s41598-019-45105-2 (2019).
22. Cha, Y., Lee, Y., Ji, E., Han, S., Min, S., Kim, H., Cho, M., Lee, H., Park, Y. & Moon, J. Y. Sustained Attention Task (gradCPT) Dataset using simultaneous EEG-fMRI and DTI. *OpenNeuro* [Dataset] doi:10.18112/openneuro.ds006040.v1.0.0
23. Noble, S. et al. Multisite reliability of MR-based functional connectivity. NeuroImage 146, 959–970 https://doi.org/10.1016/j.neuroimage.2016.10.020 (2017).
24. Kuroda, T. *et al.* Test-retest reliability of EEG microstate metrics for evaluating noise reductions in simultaneous EEG-fMRI. *Imaging Neuroscience* **2**, 1–20 https://doi.org/10.1162/imag_a_00272 (2024).
25. Gorgolewski, K. J. *et al.* The brain imaging data structure, a format for organizing and describing outputs of neuroimaging experiments. *Sci. Data* **3**, 1–9 https://doi.org/10.1038/sdata.2016.44 (2016).
26. Pernet, C. R. et al. EEG-BIDS, an extension to the brain imaging data structure for electroencephalography. *Sci. Data* **6**, 103 https://doi.org/10.1038/s41597-019-0104-8 (2019).
27. Delorme, A. & Makeig, S. EEGLAB: an open source toolbox for analysis of single-trial EEG dynamics including independent component analysis. J. *Neurosci. Methods* **134**, 9–21 https://doi.org/10.1016/j.jneumeth.2003.10.009 (2004).
28. Jas, M., Engemann, D. A., Bekhti, Y., Raimondo, F. & Gramfort, A. Autoreject: Automated artifact rejection for MEG and EEG data. *NeuroImage* **159**, 417–429 https://doi.org/10.1016/j.neuroimage.2017.06.030 (2017).
29. Bigdely-Shamlo, N., Mullen, T., Kothe, C., Su, K.-M. & Robbins, K. A. The PREP pipeline: standardized preprocessing for large-scale EEG analysis. *Front. Neuroinform.* **9**, https://doi.org/10.3389/fninf.2015.00016 (2015).
30. Niazy, R. K., Beckmann, C. F., Iannetti, G. D., Brady, J. M. & Smith, S. M. Removal of FMRI environment artifacts from EEG data using optimal basis sets. *Neuroimage* **28**, 720–737 https://doi.org/10.1016/j.neuroimage.2005.06.067 (2005).

31. Iannetti, G. D. *et al.* Simultaneous recording of laser-evoked brain potentials and continuous, high-field functional magnetic resonance imaging in humans. *Neuroimage* **28**, 708–719 https://doi.org/10.1016/j.neuroimage.2005.06.060 (2005).
32. Esteban, O. *et al.* fMRIPrep: a robust preprocessing pipeline for functional MRI. *Nat Methods* **16**, 111–116 https://doi.org/10.1038/s41592-018-0235-4 (2019).
33. Tanaka, C. S. et al. A multi-site, multi-disorder resting-state magnetic resonance image database. *Sci. data* **8**, 227 https://doi.org/10.1038/s41597-021-01004-8 (2021).
34. Alfaro-Almagro, F. *et al.* Image processing and Quality Control for the first 10,000 brain imaging datasets from UK Biobank. *NeuroImage* **166**, 400–424 https://doi.org/10.1016/j.neuroimage.2017.10.034 (2018).
35. Pernet C. Archiving and Sharing Functional MRI data. *fMRI data sharing verision 2*. Edinburgh Imaging, University of Edinburgh. https://doi.org/10.7488/ds/1347. (2016).
36. Tsutsumi, M., Kishi, T., Ogawa, T., Kuroda, T., Kobler, J. R., Kawanabe, An EEG-fMRI dataset with carbon wire loops in cognitive tasks and resting state (atr-EfP-2025) https://doi.org/10.34860/atr-EfP-2025 (2025).
37. Scharinger, C., Soutschek, A., Schubert, T., & Gerjets, P. Comparison of the Working Memory Load in N-Back and Working Memory Span Tasks by Means of EEG Frequency Band Power and P300 Amplitude. *Front. Hum. Neurosci.*, **11**, 6 https://doi.org/10.3389/fnhum.2017.00006 (2017).
38. Harsay, H. A., Spaan, M., Wijnen, J. G., Ridderinkhof, K. R. Error awareness and salience processing in the oddball task: Shared neural mechanisms. *Front. Hum. Neurosci*, **6**, 246. https://doi.org/10.3389/fnhum.2012.00246. (2012).
39. Yaple, A. Z., Stevens, D. W., & Arsalidou, M. Meta-analyses of the n-back working memory task: fMRI evidence of age-related changes in prefrontal cortex involvement across the adult lifespan. *Neuroimage*, **196**, 16-31 https://doi.org/10.1016/j.neuroimage.2019.03.074 (2019).

Acknowledgements

We thank Tomosumi Haitani, Issaku Kawashima, Tomoko Kawashima and Kana Inoue for help of data collection; Miki Kitagawa preparing for the experiment; Yoko Matsumoto for recruiting participants and scheduling the experiment. Furthermore, we would like to thank the team from the ATR Brain Activity Imaging Center (BAIC), in particular, Akikazu Nishikido, Nobuyoshi Tanki, and Akihide Yamamoto for their technical support.

Funding

This work was supported by Innovative Science and Technology Initiative for Security Grant Number JPJ004596, ATLA, Japan.

Author contributions

Mizuki Tsutsumi and Tomohiko Kishi collected, analyzed, and interpreted the data and drafted the manuscript. They are equal contributors to this work and are designated as co-first authors. Takeshi Ogawa and Toshikazu Kuroda collected data and advised on data analysis and interpretation. Reinmar J. Kobler developed the EEG preprocessing pipeline. Takeshi Ogawa, Toshikazu Kuroda, and Reinmar J. Kobler contributed to the study conception and design under the supervision of Motoaki Kawanabe. All authors read and approved the final manuscript.

Competing interests

We have no conflict of interest.

Figure legends

Fig. 1 PSD in each step of preprocessing. The solid line represents the mean, while the light-colored bands indicate ±1 standard deviation. GA refers to gradient artifact correction (steps 1–4, 6, and 7 in Table 3). EEG-fMRI (preprocessed) represents the combination of gradient artifact (GA) correction (steps 1–4, 6, and 7 in Table 3) and CWL regression (steps 1–7 in Table 3). EEG-fMRI with autoreject includes gradient artifact correction, CWL regression, artifact removal using *autoreject*, and other noise reduction methods (all steps). EEG-only (preprocessed) refers to the application of steps 1, 3, and 6 in Table 3, while EEG-only with autoreject represents the application of steps 1, 3, 6, and 8–13 in Table 3. The slight increase in PSD at 60 Hz for EEG-only reflects the alternating current (AC) power supply in Western Japan, where the experiment was conducted. CWL: Carbon wire loop, EEG: Electroencephalogram, GA: Gradient artifact, PSD: Power spectral density

Fig. 2 Traces of all EEG channels for a representative participant during the 5 seconds from 60 seconds

after resting state task measurement in Prisma on Day 1 begins. GA refers to gradient artifact correction (steps 1–4, 6, and 7 in Table 3). EEG-fMRI (preprocessed) represents the combination of gradient artifact (GA) correction (steps 1–4, 6, and 7 in Table 3) and CWL regression (steps 1–7 in Table 3). EEG-only (preprocessed) refers to the application of steps 1, 3, and 6 in Table 3. GA: Gradient artifact, CWL: Carbon wire loop.

Fig. 3 ERPs in the oddball task for Prisma, averaged across subjects. Thick vertical lines represent the onset of normal or target stimuli, detected by photo sensors. Dashed vertical lines indicate 200–400 ms in steps of 50 ms after the stimulus onset, corresponding to topography maps above each ERP graph. Each line corresponds to an electrode (Fz: cyan, Cz: orange, Pz: green, Oz: magenda, and others: gray), each referenced to the mean microvolt between -100 and 0 ms relative to the stimulus onset. The colored electrodes on the topography correspond to the electrodes showing ERP waveforms of the same color. (**A**)Trials with target stimuli for simultaneous EEG-fMRI; (**B**)Trials with normal stimuli for simultaneous EEG-fMRI; (**C**) Trials with target stimuli for EEG-only; (**D**)Trials with normal stimuli for EEG-only. EEG-fMRI with autoreject includes GA correction, CWL regression, artifact removal using autoreject, and other noise reduction methods (all steps in Table 3). EEG-only with autoreject represents the application of steps 1, 3, 6, and 8–13 in Table 3. CWL: carbon wire loop; ERP: event-related potential; GA: gradient artifact.

Fig. 4 ERPs in the oddball task for Verio, averaged across subjects. See Fig. 3 for details.

Fig. 5 ERPs in the N-back task for Prisma, averaged across subjects. Thick vertical lines represent the onset of match or non-match stimuli, detected by photo sensors. Dashed vertical lines indicate 200–400 ms in steps of 50 ms after the stimulus onset, corresponding to topography maps above each ERP graph. Each line corresponds to an electrode (Fz: cyan, Cz: orange, Pz: green, Oz: magenda, and others: gray), each referenced to the mean microvolt between -100 and 0 ms relative to the stimulus onset. The colored electrodes on the topography correspond to the electrodes showing ERP waveforms of the same color. (**A**)Trials with match stimuli (0-back) for simultaneous EEG-fMRI; (**B**) Trials with non-match stimuli (0-back) for simultaneous EEG-fMRI; (**C**) Trials with match stimuli (0-back) for EEG-only. (**D**) Trials with non-match stimuli (0-back) for EEG-only ; (**E**) Trials with match stimuli (2-back) for simultaneous EEG-fMRI; (**F**) Trials with non-match stimuli (2-back) for simultaneous EEG-fMRI; (**G**)

Trials with match stimuli (2-back) for EEG-only; (**H**) Trials with non-match stimuli (2-back) for EEG-only. EEG-fMRI with autoreject includes GA correction, CWL regression, artifact removal using autoreject, and other noise reduction methods (all steps in Table 3). EEG-only with autoreject represents the application of steps 1, 3, 6, and 8–13 in Table 3. CWL: carbon wire loop; ERP: event-related potential; GA: gradient artifact.

Fig. 6 ERPs in the N-back task for Verio, averaged across subjects. See Fig. 5 for details.

Table legends

Table.2 Notes: We did not conduct visual oddball and N-back tasks in Verio on Day 2 for conducting a different experimental task as part of collaborative research with a different laboratory, which was outside the scope of the present study.

Table 5. Notes: The MNI coordinate corresponds to the peak voxels within each cluster. Clusters were set at a threshold of $p < 0.001$ and the cluster level family-wise-error was set at $p < 0.05$. Notes: Brain regions were labelled by the AAL toolbox in the SPM extension. IOG: Inferior occipital gyrus, CER6: Lobule VI of cerebellar hemisphere, MTG: Middle temporal gyrus, SMA: Supplementary motor area, IPG: Inferior parietal gyrus, excluding supramarginal and angular gyri, PoCG: Postcentral gyrus, SMG: SupraMarginal gyrus, MOG: Middle occipital gyrus, CER7b: Lobule VIIB of cerebellar hemisphere, CER8: Lobule VIII of cerebellar hemisphere, CAU: Caudate nucleus, REC: Gyrus rectus, INS: Insula, MFG: Middle frontal gyrus

Table 6. Notes: The MNI coordinate corresponds to the peak voxels within each cluster. Clusters were set at a threshold of $p < 0.001$ and the cluster level family-wise-error was set at $p < 0.05$. Notes: Brain regions were labelled by the AAL toolbox in the SPM extension. PoCG: Postcentral gyrus, PreCG: Precentral gyrus, CER6: Lobule VI of cerebellar hemisphere, MFG: Middle frontal gyrus, ROL: Rolandic operculum, CER4_5: Lobule IV, V of cerebellar hemisphere, CER8: Lobule VIII of cerebellar hemisphere, IFGorb: IFG pars orbitalis, INS: Insula, STG: Superior temporal gyrus, ITG: Inferior temporal gyrus, MTG: Middle temporal gyrus, IPG: Inferior parietal gyrus, IFGtriang: Inferior frontal gyrus, triangular part

Table 7. Notes: The MNI coordinate corresponds to the peak voxels within each cluster. Clusters were set at a threshold of $p < 0.001$ and the cluster level family-wise-error was set at $p < 0.05$. Notes: Brain regions were labelled by the AAL toolbox in the SPM extension. SMA: Supplementary motor area, SFG: Superior frontal gyrus, dorsolateral, PAL: Lenticular nucleus, Pallidum, IFGorb: IFG pars orbitalis, IFGtriang: Inferior frontal gyrus, triangular part, PoCG: Postcentral gyrus, PreCG: Precentral gyrus, MOG: Middle occipital gyrus, FFG: Fusiform gyrus, IOG: Inferior occipital gyrus, SOG: Superior occipital gyrus, CAL: Calcarine fissure and surrounding cortex, IPG: Inferior parietal gyrus, excluding supramarginal and angular gyri, SPG: Superior parietal gyrus, MFG: Middle frontal gyrus , CER6: Lobule VI of cerebellar hemisphere, CERCRU1: Crus I of cerebellar hemisphere

Table 8. The MNI coordinate corresponds to the peak voxels within each cluster. Clusters were set at a threshold of $p < 0.001$ and the cluster level family-wise-error was set at $p < 0.05$. Notes: Brain regions were labelled by the AAL toolbox in the SPM extension. PUT: Lenticular nucleus, Putamen, CER6: Lobule VI of cerebellar hemisphere, MCC: Middle cingulate & paracingulate gyri, PoCG: Postcentral gyrus, SMG: SupraMarginal gyrus, LING: Lingual gyrus, CAL: Calcarine fissure and surrounding cortex, SOG: Superior occipital gyrus, ANG: Angular gyrus, SFG: Superior frontal gyrus, dorsolateral, MFG: Middle frontal gyrus, PreCG: Precentral gyrus, CAU: Caudate nucleus, PAL: Lenticular nucleus, Pallidum, ACC: Anterior cingulate & paracingulate gyri, SFGmedial: Superior frontal gyrus, medial, CER4_5: Lobule IV, V of cerebellar hemisphere, ROL: Rolandic operculum, THA: Thalamus, INS: Insula, STG: Superior temporal gyrus, MTG: Middle temporal gyrus

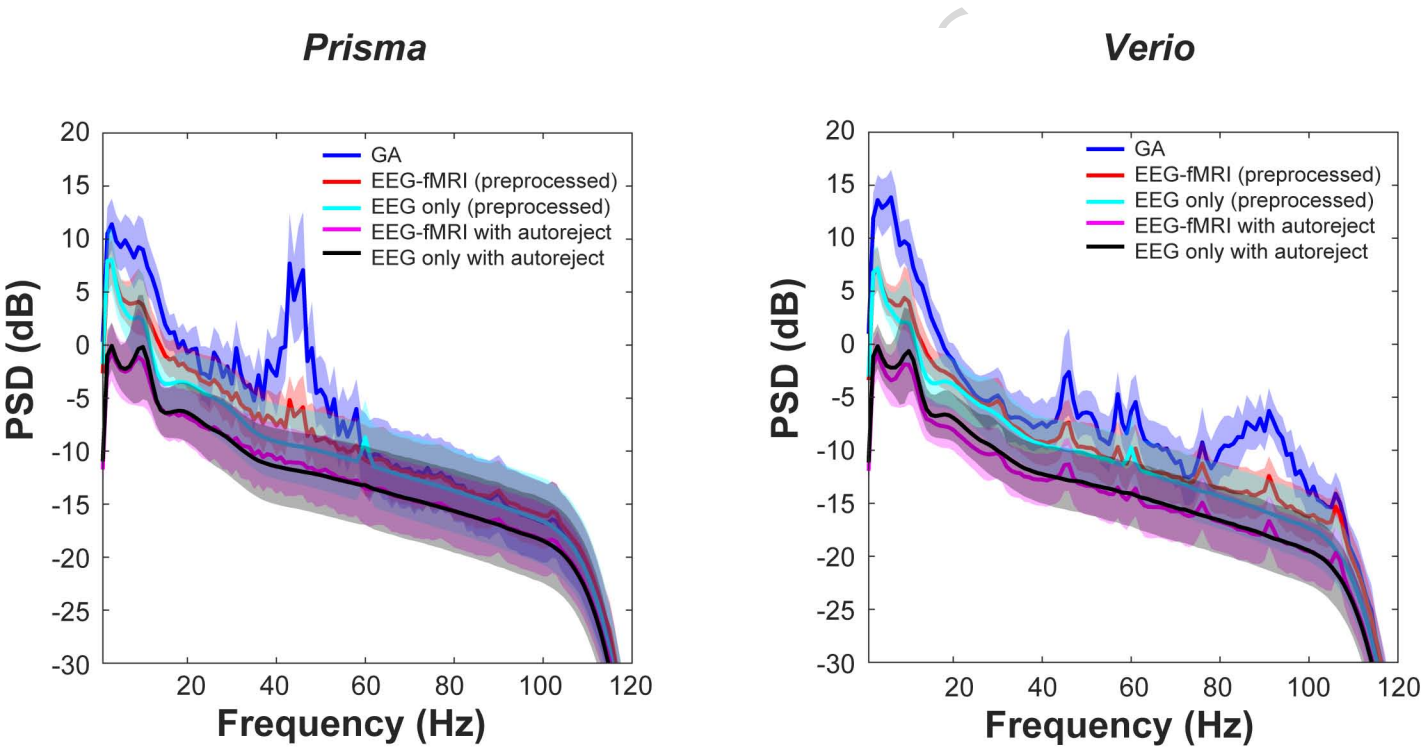
Prisma
Verio
GA
EEG-fMRI (preprocessed)
EEG only (preprocessed)
EEG-fMRI with autoreject
EEG only with autoreject
PSD (dB)
Frequency (Hz)
20
15
10
5
0
-5
-10
-15
-20
-25
-30
20
40
60
80
100
120

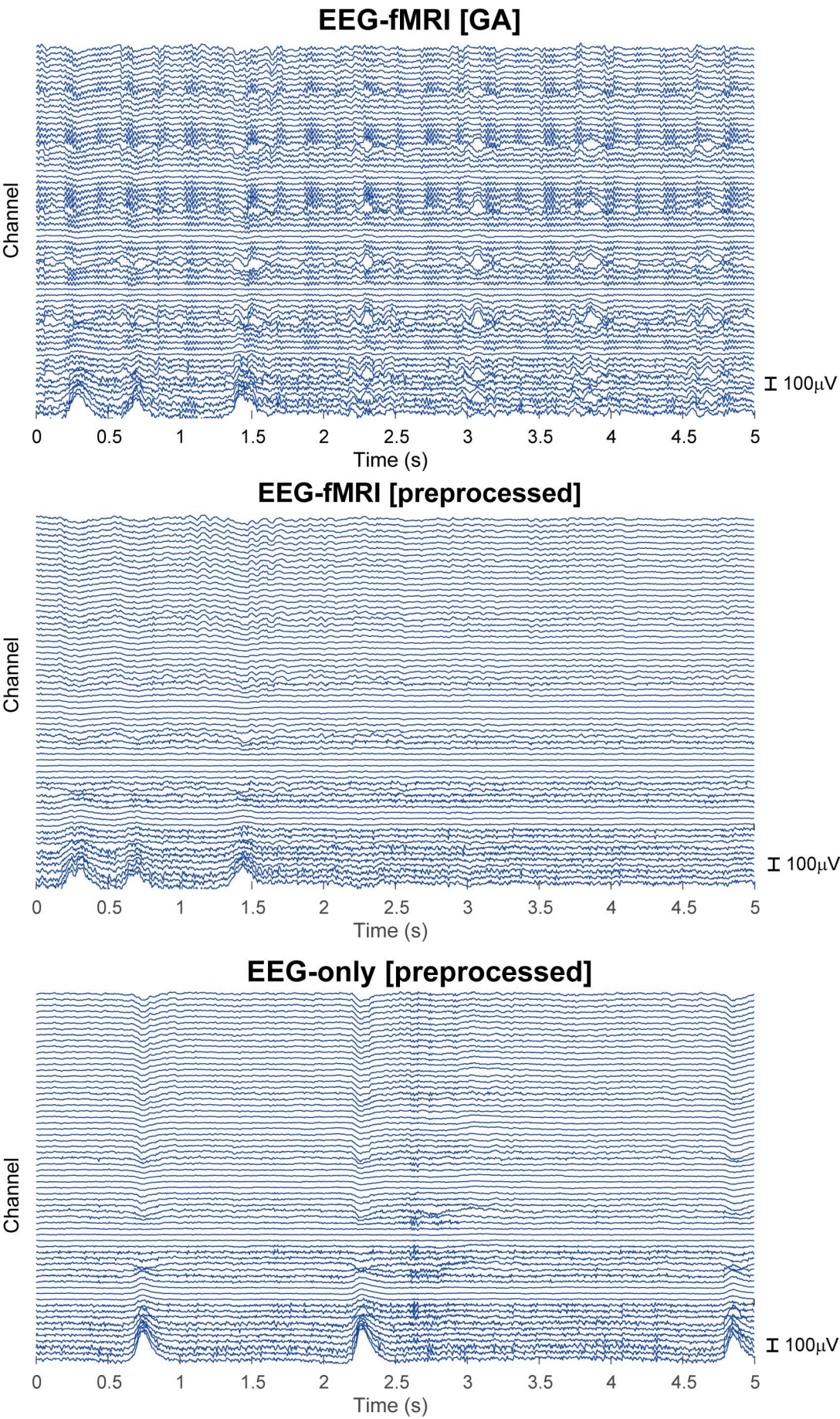
EEG-fMRI [GA]
Channel
100μV
0
0.5
1
1.5
2
2.5
3
3.5
4
4.5
5
Time (s)
EEG-fMRI [preprocessed]
Channel
100μV
0
0.5
1
1.5
2
2.5
3
3.5
4
4.5
5
Time (s)
EEG-only [preprocessed]
Channel
100μV
0
0.5
1
1.5
2
2.5
3
3.5
4
4.5
5
Time (s)

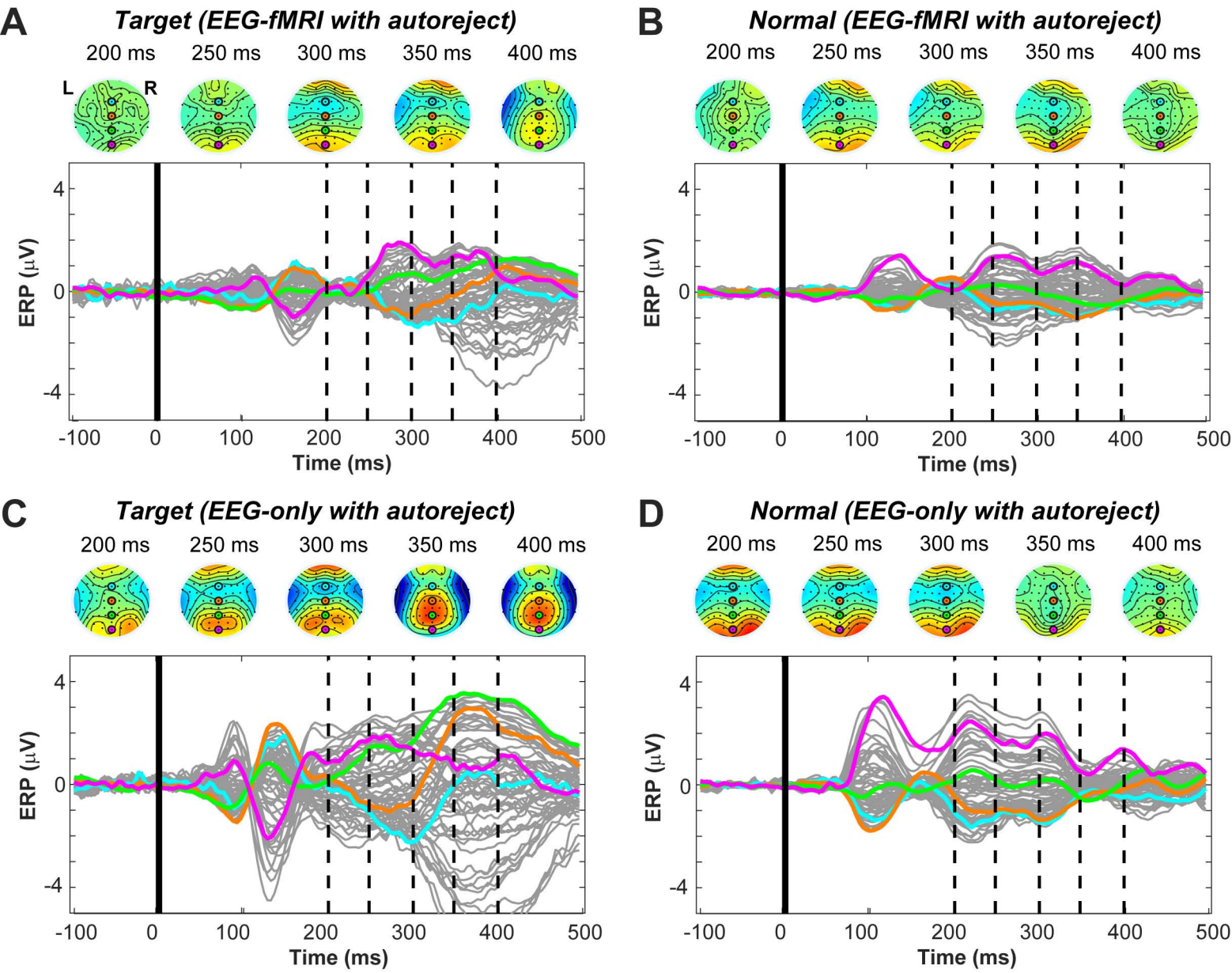
A
Target (EEG-fMRI with autoreject)
200 ms
250 ms
300 ms
350 ms
400 ms
L
R
ERP (μV)
Time (ms)
B
Normal (EEG-fMRI with autoreject)
C
Target (EEG-only with autoreject)
D
Normal (EEG-only with autoreject)

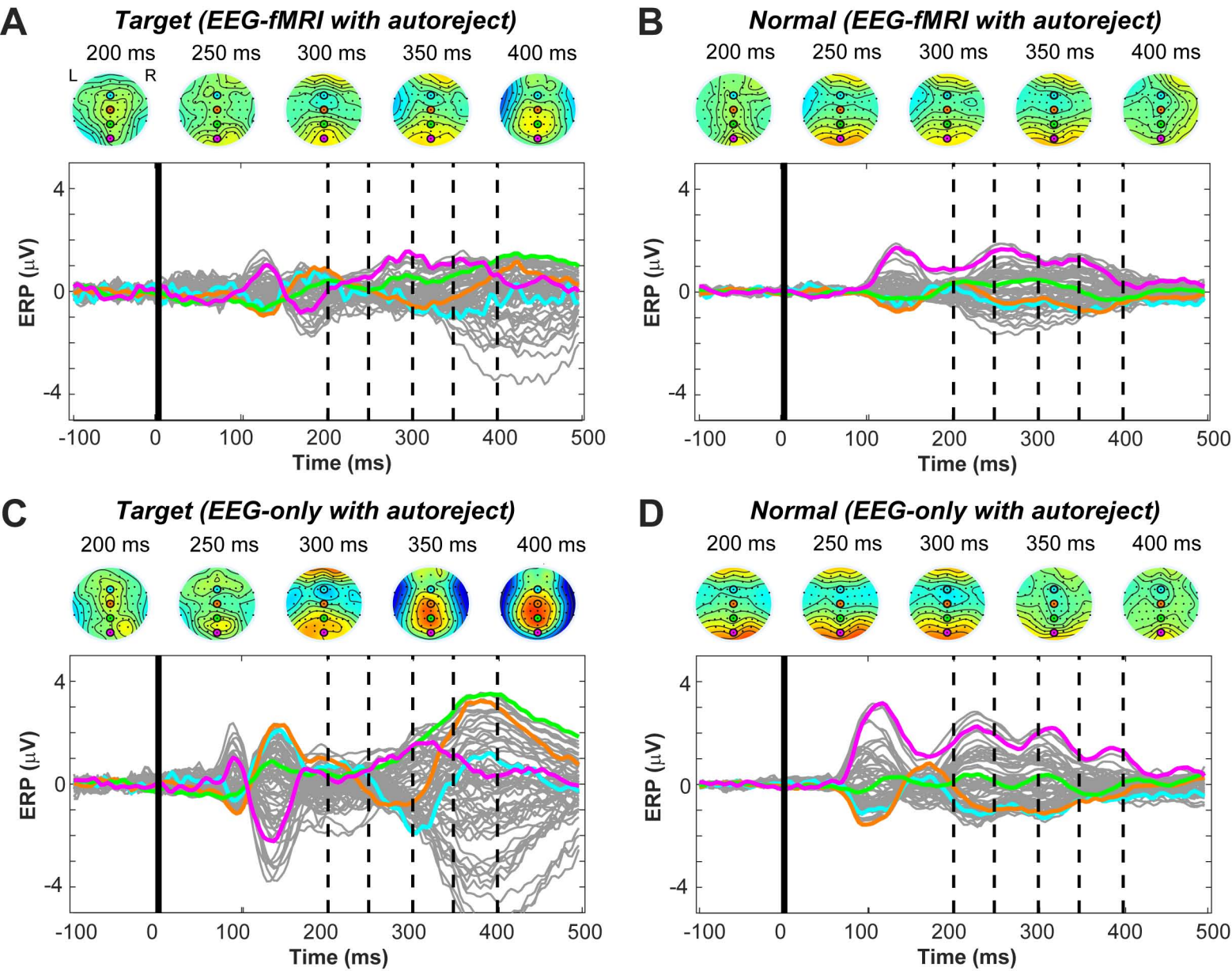
A
Target (EEG-fMRI with autoreject)
200 ms
250 ms
300 ms
350 ms
400 ms
L
R
ERP (μV)
Time (ms)
B
Normal (EEG-fMRI with autoreject)
C
Target (EEG-only with autoreject)
D
Normal (EEG-only with autoreject)

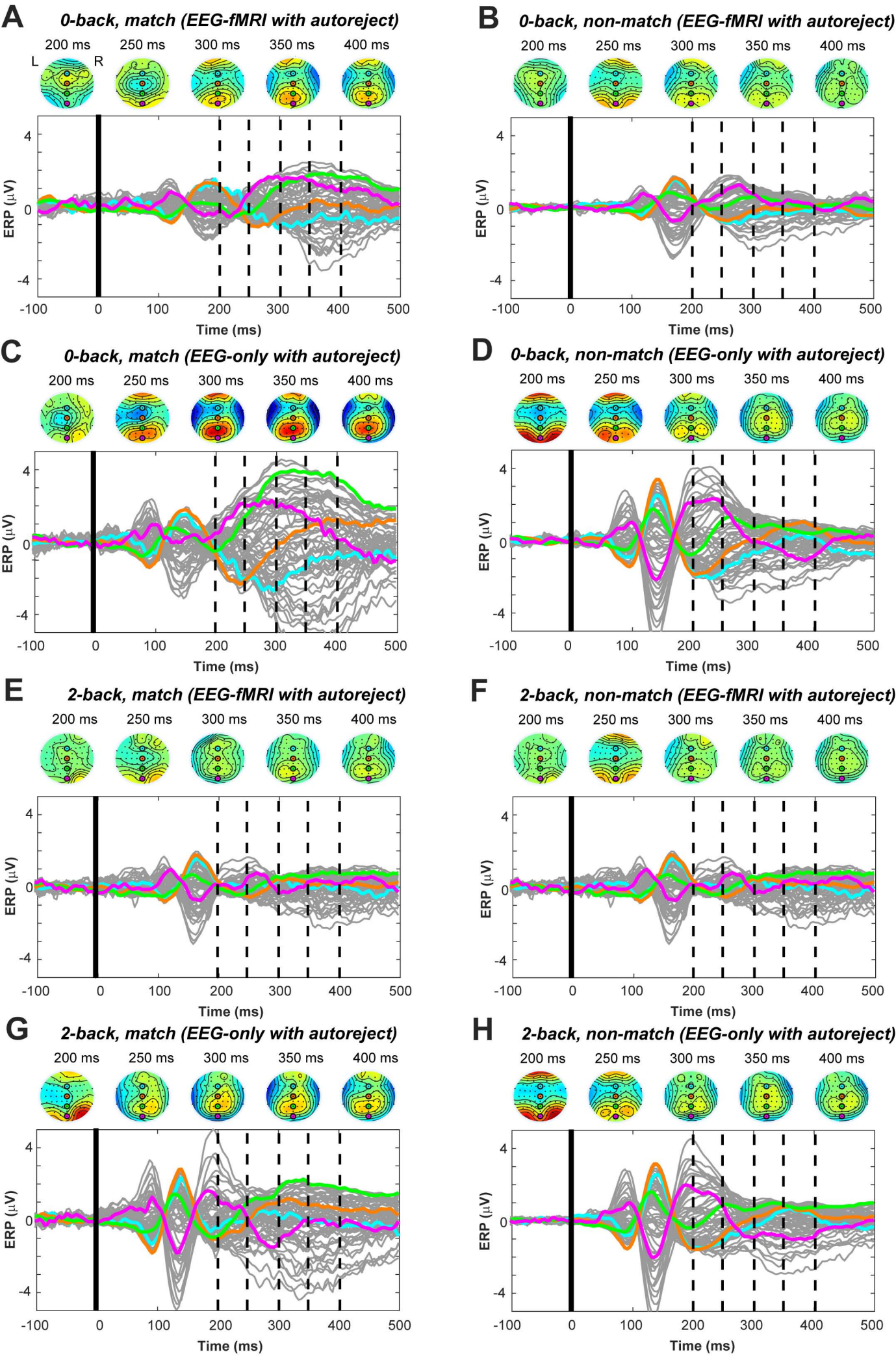
A
0-back, match (EEG-fMRI with autoreject)
B
0-back, non-match (EEG-fMRI with autoreject)
C
0-back, match (EEG-only with autoreject)
D
0-back, non-match (EEG-only with autoreject)
E
2-back, match (EEG-fMRI with autoreject)
F
2-back, non-match (EEG-fMRI with autoreject)
G
2-back, match (EEG-only with autoreject)
H
2-back, non-match (EEG-only with autoreject)
200 ms
250 ms
300 ms
350 ms
400 ms
L
R
ERP (μV)
Time (ms)

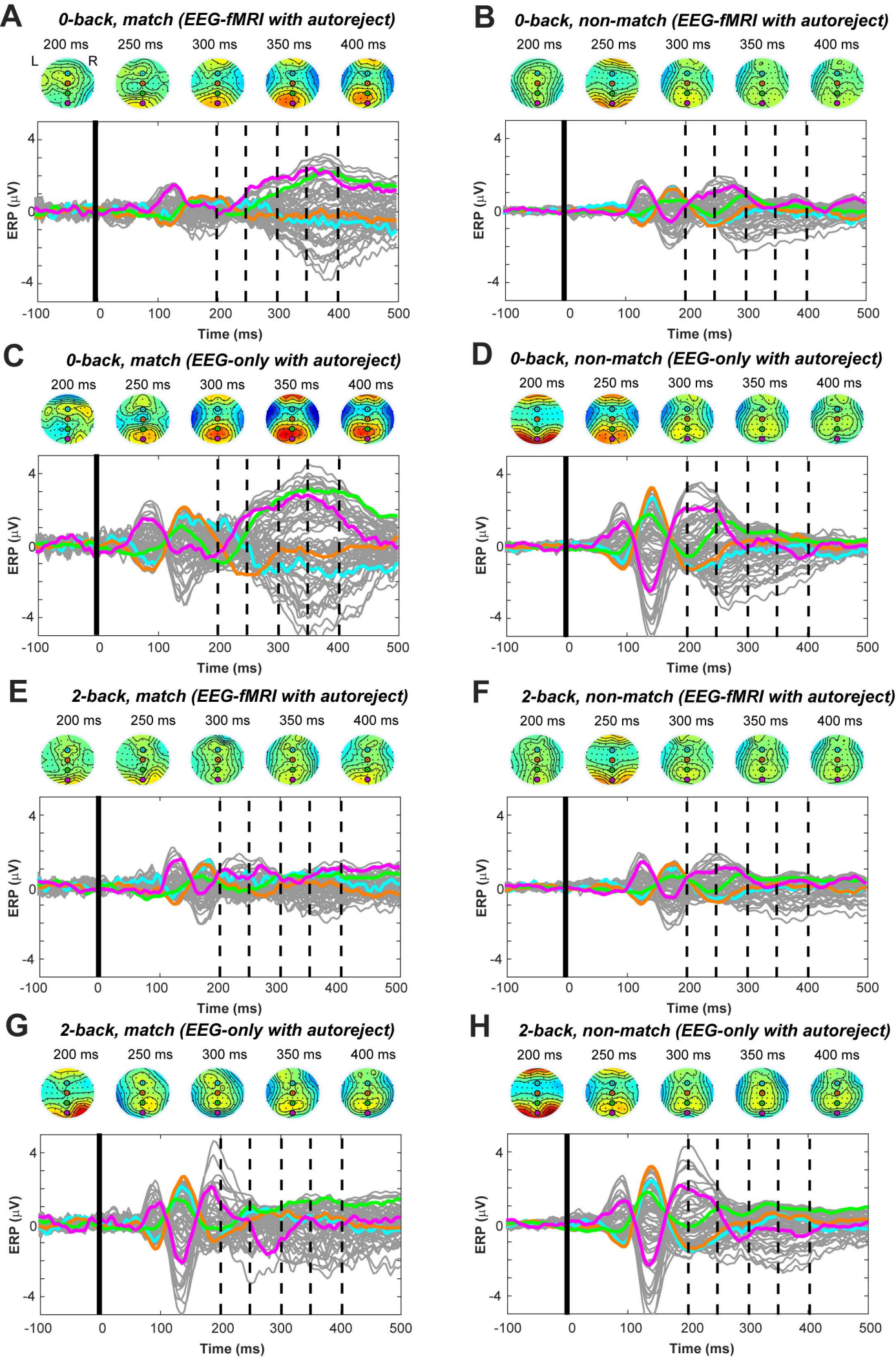
A
0-back, match (EEG-fMRI with autoreject)
B
0-back, non-match (EEG-fMRI with autoreject)
C
0-back, match (EEG-only with autoreject)
D
0-back, non-match (EEG-only with autoreject)
E
2-back, match (EEG-fMRI with autoreject)
F
2-back, non-match (EEG-fMRI with autoreject)
G
2-back, match (EEG-only with autoreject)
H
2-back, non-match (EEG-only with autoreject)
200 ms
250 ms
300 ms
350 ms
400 ms
L
R
ERP (μV)
Time (ms)